ACS APPLIED BIO MATERIALS
Cite This: ACS Appl. Bio Mater. 2018, 1, 1286−1293
Article
www.acsabm.org

Antiviral Activity of Graphene Oxide−Silver Nanocomposites by Preventing Viral Entry and Activation of the Antiviral Innate Immune Response

Ting Du,[†,∥] Jian Lu,[†,∥] Lingzhi Liu,[†] Nan Dong,[‡] Liurong Fang,[‡] Shaobo Xiao,[‡] and Heyou Han*[,†]

[†]State Key Laboratory of Agricultural Microbiology, College of Food Science and Technology, College of Science, Huazhong Agricultural University, Wuhan 430070, People's Republic of China

[‡]State Key Laboratory of Agricultural Microbiology, College of Veterinary Medicine, Huazhong Agricultural University, Wuhan 430070, People's Republic of China

Supporting Information

ABSTRACT: Developing nanomaterials-based antimicrobial agents has shown a widespread promise. In this study, silver nanoparticle-modified graphene oxide (GO-AgNPs) nanocomposites were self-assembled via interfacial electrostatic force. By using the porcine reproductive and respiratory syndrome virus (PRRSV) as a pattern, the antiviral effect of the as-prepared GO-AgNPs nanocomposites on the replication of virus was investigated. The results indicated that exposure with GO-AgNPs nanocomposites could obviously suppress PRRSV infection. It was found that GO-AgNPs nanocomposites exhibited a better inhibitory effect compared with AgNPs and GO. By selecting the porcine epidemic diarrhea virus (PEDV) as a contrast virus, GO-AgNPs nanocomposites were proven to have a broad antiviral activity. Mechanism studies showed that GO-AgNPs nanocomposites might prevent PRRSV from entering the host cells, with 59.2% inhibition efficiency. Meanwhile, GO-AgNPs nanocomposite treatment enhances the production of interferon-α (IFN-α) and IFN-stimulating genes (ISGs), which can directly inhibit the proliferation of virus. Taken together, this study reports a new type of antiviral agent and provides a promising pharmaceutical agent for treating infection by the highly pathogenic PRRSV. Moreover, it may provide novel ideas for the research and development of antiviral formulations based on nanocomposites and extend their applications in biological systems.

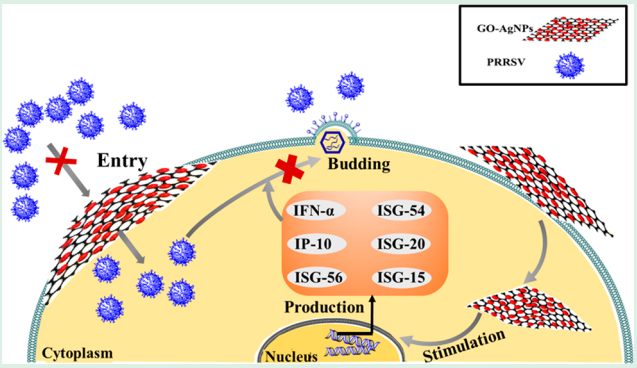

KEYWORDS: *GO-AgNPs nanocomposites, antiviral, entry, interferon-α, interferon-stimulating genes*

1. INTRODUCTION

By combining nanotechnology with biotechnology, nanomaterials possessing unique physicochemical properties have shown outstanding advantages in the field of medicine.[1] So far, a variety of nanomaterials, including carbon-based nanomaterials,[2−4] silver nanoparticles,[5,6] functional gold nanoparticles,[7−9] silicon nanoparticles,[10] and polyvalent nanoarchitectures,[11,12] have been proven to possess antiviral properties. Among these materials, metal nanoparticles have attracted great attention due to their broad-spectrum antiviral activity and inability to cause viral resistance.[13]

Silver nanoparticles (AgNPs), as a member of noble metal nanomaterials, have gained considerable attention due to their excellent antibacterial, antifungal, and antiviral properties.[14−16] Baram et al. have reported that mercaptoethanesulfonate (MES)-capped AgNPs can suppress viral infection by blocking the viral attachment, thereby prohibiting the cell-to-cell infection.[17] Lu et al. have found that AgNPs with different sizes can inhibit hepatitis B virus (HBV) replication and extracellular virions by their high affinity with viral dsDNA.[18] Many researches have suggested that the size, shape, stability and capping agents made a big difference in efforts in the antiviral effect of AgNPs.[19] However, naked AgNPs are easily agglomerated due to their high reactivity, which will reduce their antimicrobial activity greatly.[20] Therefore, a variety of organic and inorganic substances are adopted as stabilizers to modify the surface of AgNPs.[21,22]

In recent years, carbon-based nanomaterials have attracted increasing attention because of the material's good biocompatibility and excellent physicochemical characteristics. Carbon-based nanomaterials, for instance, GO, carbon dots (CDs), and fullerenes, have been proven to have a strong antiviral activity.[23−25] As one of the most important members of carbon-based nanomaterials, GO nanosheets with two-dimen-

Received: May 24, 2018
Accepted: October 30, 2018
Published: October 30, 2018

DOI: 10.1021/acsabm.8b00154
ACS Appl. Bio Mater. 2018, 1, 1286−1293

sional morphologies were considered to be a promising viral inhibitor. For example, Ye et al. proved that GO and its derivatives have antiviral properties due to their extraordinary nanosheet structure and negative charge.[23] Sametband et al. prepared a graphene oxide derivative (rGO−SO_3) by simulating the cell surface receptor heparan sulfate and demonstrated that this composite can inhibit HSV-1 infection.[24] Huang et al. constructed multifunctionalized GO composites and demonstrated that the composites could prevent respiratory syncytial virus (RSV) infection through immediately inactivating the virus and suppressing adhesion.[26] In addition, GO sheets own rich polar oxygen functional groups in its aromatic plane that can support DNA,[27] metal oxides,[28] polymers,[29] and inorganic nanoparticles.[30]

In our recent work, GO/g-C_3N_4 nanocomposites have been successfully constructed. The photocatalytic bactericidal activity of GO/g-C_3N_4 was greatly enhanced by introducing GO.[31] The inhibition efficiency of GO-AgNPs nanocomposites on phytopathogen *Fusarium graminearum* showed a remarkable enhancement when compared with GO and AgNPs.[32]

The above results revealed that the combination of GO with other nanomaterials may provide enhanced antimicrobial activity. Considering the strong antiviral activity of AgNPs and GO, herein, GO-AgNPs nanocomposites were constructed and their antiviral activity was investigated. It can be expected that GO-AgNPs nanocomposites would have a better inhibitory effect than AgNPs and GO. As we have seen, the potential inhibitory influence of GO-AgNPs nanocomposites on a virus is rarely reported, and the mechanism of their impact on the virus remains to be explored.

Porcine reproductive and respiratory syndrome virus (PRRSV) is a single-stranded positive-sense RNA virus, which posed a huge threat to the pig industry and brought considerable financial ruin to the global livestock industry.[33] Therefore, in this study, PRRSV was selected as an RNA virus model to evaluate the inhibitory effect of GO-AgNPs nanocomposites. It was found that GO-AgNPs nanocomposites might inhibit viral invasion of the host cells and thus inhibiting the viral replication. In addition, GO-AgNPs nanocomposites might also inhibit the multiplication of PRRSV by activating antiviral natural responses.

2. EXPERIMENTAL SECTION

2.1. Preparation of GO and AgNPs. GO nanosheets were prepared by the sonication of commercially available graphene oxide.[34] The synthesis of AgNPs was based on previous reports, and some minor modifications have been made.[35] $AgNO_3$ (25 mL/1.0 mM) solution was injected dropwise into $NaBH_4$ (75 mL/2 mM) solution under vigorous stirring, followed by adding 5.0 mL of 1 wt % citrate and stirring together for the specified time (15 min). The resulting AgNPs were filtered and centrifugated at 8000 rpm. Finally, the sediment was collected, resuspended in deionized water, and stored at 4 °C.

2.2. Synthesis of GO-AgNPs Nanocomposites. PVP-capped GO was obtained via adding 80 mg of PVP to 20 mL of GO solution. The hydrophobic side of PVP interacts with the hydrophobic group of GO, while the exposed hydrophilic side serves the purpose of improving the hydrophilicity and dispersibility of GO. The above mixture was subjected to centrifugation after mixing for 30 min and then was dispersed in 5.0 mL of ultrapure water. PDDA-functionalized GO was obtained by the addition of PDDA (0.1 mL/20 wt %) into KCl (15 mL/0.625 M) and then the addition of 5.0 mL of PVP-capped GO. The resultant solution was subjected to ultrasonication for 1.5 h, and then the impurities were removed by centrifugation. At last, the PDDA-GO was resuspended in 2.0 mL of ultrapure water to form the ultimate concentration of 2.0 mg/mL suspension. The GO-AgNPs nanocomposites were prepared according to previous reports.[36] Typically, 1.0 mL of PDDA-GO suspension was injected into the aforementioned AgNPs (30 mL) while stirring; then ultrasonic treatment was performed for 5 min, and the mixture was kept overnight. Then the sediment was rinsed and redispersed in ultrapure water for later use.

2.3. Viral Plaque Assay. The PRRSV plaque assay was conducted on MARC-145 cells.[37] Briefly, infection of MARC-145 cells close to all confluence was achieved with a 10-fold dilution of PRRSV-containing inoculum (800 μL/well). After infection of 1 h, the cell monolayers were subjected to rinsing and then were covered with Bacto agar (1.8%) blended with 2 × DMEM (at a 1:1 ratio) containing 3% FBS. Finally, plaques were counted at 48−72 h post infection. The viral titers were shown in plaque-forming units (PFU/mL).

2.4. One-Step Growth Curves. MARC-145 cells (1.25×10^5/well) were incubated to a full monolayer, followed by incubation with DMEM (2% FBS) and GO-AgNPs nanocomposites (4.0 μg/mL) (37 °C, 2 h). Then cells were infected with PRRSV at a multiplicity of infection (MOI) of 1.0 (37 °C, 1 h). Then the control DMEM or GO-AgNPs nanocomposites were added for further incubation. Cell samples including progeny PRRSV were harvested at 1, 3, 6, 9, 12, 24, 36, and 48 h after infection and stored at −80 °C. To completely release the infectious intracellular virus, cells were treated with two freeze−thaw cycles. The titer of collected virions was calculated via the plaque assay.[38]

2.5. Virus Entry Assay. PRRSV was pretreated with GO-AgNPs nanocomposites for 1 h with 5% CO_2 at 37 °C. Then the mixture was cocultured with MARC-145 cells at 37 °C to activate the virus invasion process (1 h), followed by washing to clear the nonentered virions. Subsequently, a 1.8% agarose overlay was injected and cultured for 2−3 days or until complete viral lysis was observed in the virus control wells.[23]

2.6. Statistical Analysis. Statistical analysis was performed according to the Student's *t* test. The $*p$ value < 0.05 and $**p$ value < 0.01 were considered statistically significance.

3. RESULTS AND DISCUSSION

3.1. Characterization of GO-AgNPs Nanocomposites. To fabricate GO-AgNPs nanocomposites, an electrostatic self-assembly technique was used. It has been reported that AgNPs synthesized with citrate were negatively charged.[35] Therefore, poly diallyldimethylammonium chloride (PDDA) was employed as a surfactant to modify GO nanosheets with a positive charge to facilitate the loading of negatively charged AgNPs. Figure 1a−c represented the morphologies of GO, AgNPs, and GO-AgNPs nanocomposites, respectively. It can be seen clearly that a great amount of AgNPs with an average particle size of 17 ± 3.4 nm was evenly loaded on the surface of GO nanosheets (Figure 1c), which was consistent with the previous study.[39] Figure 1d displayed the UV−visible absorption spectra of GO, AgNPs, and GO-AgNPs nanocomposites. The maximum absorption peak of GO was found to be 230 nm, while that of AgNPs was about 410 nm.[40] Owing to the existence of surface plasmon on AgNPs, the absorption spectrum of GO-AgNPs nanocomposites indicated an obvious red shift, suggesting the successful loading of AgNPs on GO nanosheets.[41]

The ζ potential measurement provides useful information for studying the electrostatic interactions. The ζ potential of GO nanosheets was −37 ± 4.0 mV, demonstrating the negative surface charge of GO that resulted from the abundant carboxyl and hydroxyl groups (Figure 1c). After modification with PDDA, the value changed from negative to positive (39 mV), suggesting the formation of positively charged PDDA-

DOI: 10.1021/acsabm.8b00154
ACS Appl. Bio Mater. 2018, 1, 1286−1293

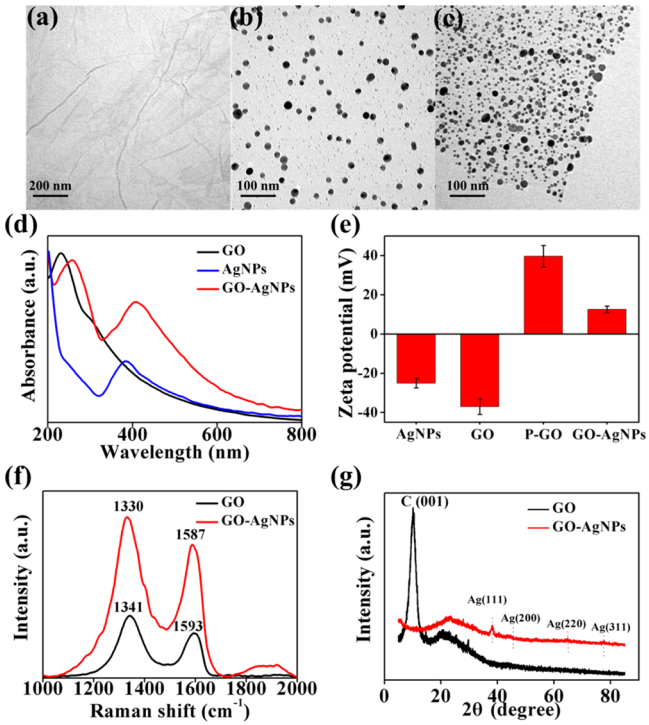

Figure 1. TEM images of GO (a), AgNPs (b), and GO-AgNPs nanocomposites (c). UV−vis spectra of GO, AgNPs, and GO-AgNPs nanocomposites (d). ζ potentials of AgNPs, GO, PDDA-GO (P-GO), and GO-AgNPs nanocomposites (e). Raman spectra (f) and XRD patterns of GO and GO-AgNPs nanocomposites (g).

GO. Dominated by an electrostatic interaction, the negatively charged AgNPs (−25 ± 2.4 mV) were electrostatically bonded to the surface of PDDA-GO and GO-AgNPs nanocomposites with a positive charge (13 ± 1.7 mV) were formed. The results of the ζ potential measurement revealed that PDDA played a key role in the process of GO-AgNPs nanocomposites formation.

Raman spectroscopy is considered to be a useful tool for detecting ordered/disordered crystalline structures of carbon nanomaterials. As presented in Figure 1f, the GO characteristic Raman bands at 1341 and 1593 cm^{-1} represent the D band and G band, respectively.[42] After electrostatic self-assembly, the peaks shifted to 1330 and 1587 cm^{-1} as a result of the surface enhanced Raman scattering (SERS). The presence of AgNPs could be verified via the XRD test. From Figure 1, it can be seen that the GO sharp peak was located in $2\theta = 10.5°$, corresponding to the GO (001) reflection. New peaks of 38.1, 45.5, 64.7, and 77.5° can be observed through the electrochemical modification with AgNPs, which can be attributed to the (111), (200), (220), and (311) faces of face-centered cubic AgNPs, thus indicating the successful fabrication of GO-AgNPs nanocomposites. It was important to note that the peak at 10.5° thoroughly disappeared after electrostatic self-assembly, which was in agreement with the literature.[43]

The full range XPS spectrum of GO distinctly presented three peaks at 285.8, 403.1, and 532.8 eV, corresponding to C 1s, N 1s, and O 1s. (Figure 2a). The existence of C—C/C═C (284.8 eV), C—OH (285.8 eV), C (epoxy) (286.7 eV), and C═O (287.8 eV) functions in C 1s by a high-resolution XPS spectrum indicated that the preparation of GO was successful (Figure 2b). Compared to pure GO, an additional Ag 3d peak at 370.2 eV appeared in the spectrum of GO-AgNPs nanocomposites, implying that the surface composition of GO has been altered by AgNPs. The two sharp peaks of 368.1 and 374.1 eV observed in Ag 3d spectra could be assigned to Ag $3d_{3/2}$ and Ag $3d_{5/2}$ photoelectrons (Figure 2e). Additionally, the peak strength of the oxygen-containing functional group was significantly lower than that of the pure GO nanosheets. The C 1s peaks of GO-AgNPs nanocomposites demonstrated that carbon was mainly presented in the shape of C—C/C═C, C—OH, and C (epoxy) (Figure 2d). The above data revealed that the surface of GO-AgNPs nanocomposites was rich in hydrophilic groups and provided them with a good water dispersibility.[44] The FT-IR spectrum of GO-AgNPs nanocomposites displayed strong and wide peaks at 3435 cm^{-1} because of the tensile vibration of O—H groups.[45] The new characteristic peaks emerged at about 2884, 1475−1300, and 650−1000 cm^{-1} could be ascribed in turn to C—H stretching vibrations and C—H in-plane and out-of-plane bending vibrations. A contribution at 1641 and 1115 cm^{-1} showed the C═C and C═O stretching and C—H bending vibration (Figure 2f). Apparently, the chemical structure of GO-AgNPs nanocomposites identified by FT-IR spectra was consistent with the results of XPS.

3.2. Effect of GO-AgNPs Nanocomposites on Cell Viability. To evaluate the potential cytotoxicity of GO-AgNPs nanocomposites, the relative survival rate of MARC-145 cells was tested. Typically, MARC-145 cells were cultured with GO-AgNPs nanocomposites for 24 and 48 h, respectively. As revealed in Figure 3, after incubation with GO-AgNPs nanocomposites (0.5−4.0 μg/mL) for 24 and 48 h, the relative survival rate of cells was all greater than 85%, suggesting the good biocompatibility of the GO-AgNPs nanocomposites. However, when the concentration was 8.0 μg/mL, the cytotoxicity was small and cell viability decreased slightly to 80%. Therefore, the following assays were carried out with a concentration of 4.0 μg/mL.

3.3. Antiviral Activity of GO-AgNPs against PRRSV. To explore the influence of GO-AgNPs nanocomposites on PRRSV, one-step growth curves were plotted to detect the changes of virus titers caused by the treatment of GO-AgNPs nanocomposites (4.0 μg/mL) during viral replication. From Figure 4, it can be found that the viral titers reduced in the existence of GO-AgNPs nanocomposites compared to the control assays, implying that GO-AgNPs nanocomposites indeed possessed anti-PRRSV infection activity.

To verify the inhibitory effect of GO-AgNPs nanocomposites on PRRSV, the expression of PRRSV N protein was detected after GO-AgNPs nanocomposite treatment. For this purpose, the exposed or unexposed cells were first cultured with PRRSV (1 h, 37 °C) and then incubated with GO-AgNPs nanocomposites (0.5−8.0 μg/mL) for 36 hpi, followed by fixation and staining with a specific antibody against PRRSV N protein. PRRSV N protein plays a variety of important functions in the process of virus infection. As demonstrated in Figure 5, the green fluorescence signal in the GO-AgNPs nanocomposite treatment group was dramatically lower than that in the blank control group, and the fluorescent signal directly reflected the expression level of N protein. It was found that the decrease of green fluorescence signal followed a dose-dependent manner. As the concentrations of GO-AgNPs nanocomposites increased, the fluorescence signal gradually reduced. As the concentration of GO-AgNPs nanocomposites reached 8.0 μg/mL, a negligible green fluorescence signal was observed, indicating the low expression level of N protein and

DOI: 10.1021/acsabm.8b00154
ACS Appl. Bio Mater. 2018, 1, 1286−1293

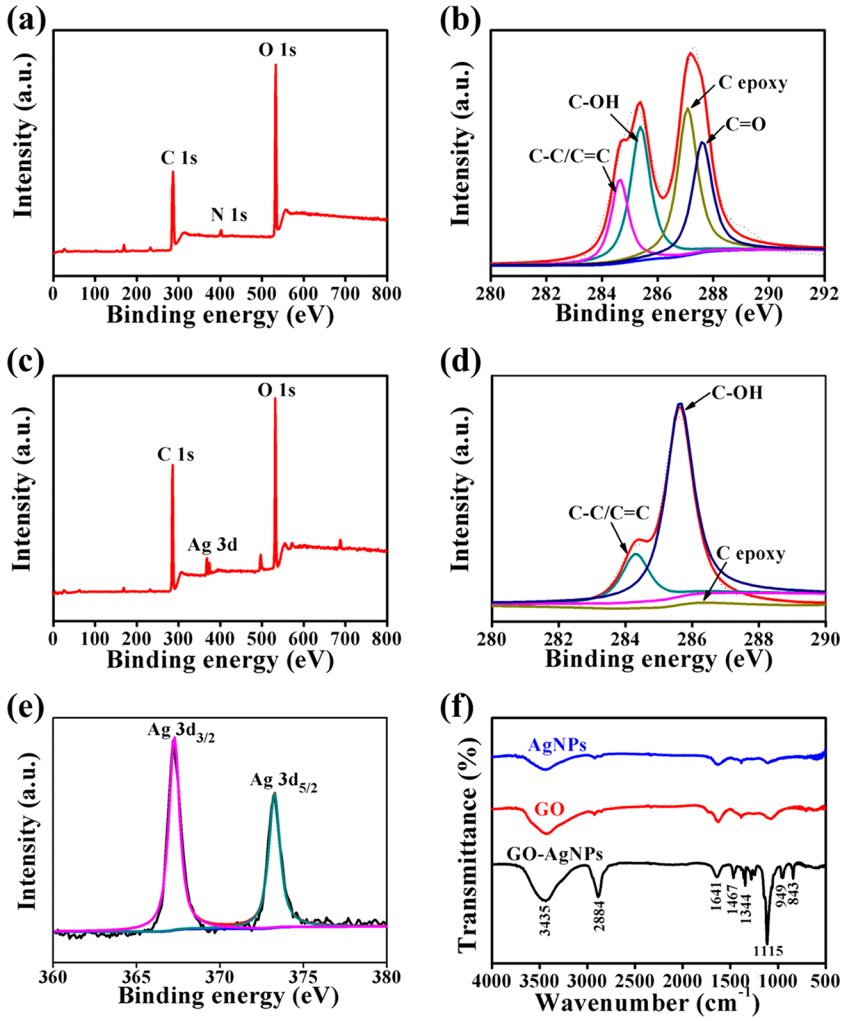

Figure 2. XPS-survey spectra of GO (a) and C 1s high-resolution survey spectrum (b). XPS spectrum of GO-AgNPs nanocomposites (c), C 1s (d), and Ag 3d (e) high-resolution survey spectra. FT-IR spectra of GO, AgNPs, and GO-AgNPs nanocomposites (f).

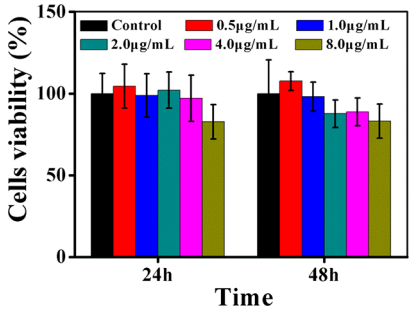

Figure 3. In vitro cytotoxicity of GO-AgNPs nanocomposites to MARC-145 cells. Cells were cultured with different concentrations of GO-AgNPs nanocomposites (0.5−8.0 μg/mL) for 24 and 48 h, respectively.

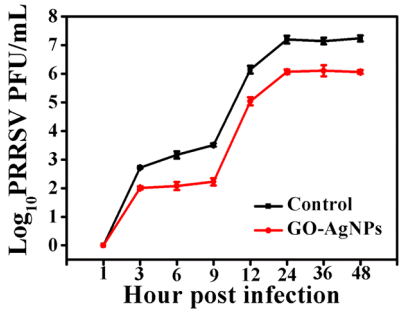

Figure 4. One-step growth curves of virus after treatment or without treatment with GO-AgNPs nanocomposites (4.0 μg/mL). Cells were infected with PRRSV (MOI = 1.0) for the indicated periods of time.

the high inhibitory activity of the nanocomposites. These results further confirmed the conclusion of one-step growth curves in Figure 4.

To further prove the inhibitory effect of GO-AgNPs nanocomposites, the antiviral activity of pure AgNPs and GO nanosheets against PRRSV was also studied. The indirect immunofluorescence assay and Western blot analysis using a viral specific antibody were regarded as intuitive and effective diagnostic tools. In brief, the same concentrations of GO, AgNPs, and GO-AgNPs nanocomposites (4.0 μg/mL) were cultured with infected MARC-145 cells for 36 hpi. Cells exposed with GO or AgNPs alone also presented a lower fluorescence signal when compared to the positive control group (Figure 6a), demonstrating that GO and AgNPs both had antiviral activities. However, the fluorescence in cells treated with GO-AgNPs nanocomposites displayed a noteworthy reduction, almost the same as the negative control group, suggesting the stronger inhibitory effect of the nanocomposites. The results revealed that the electrostatic

DOI: 10.1021/acsabm.8b00154
ACS Appl. Bio Mater. 2018, 1, 1286−1293

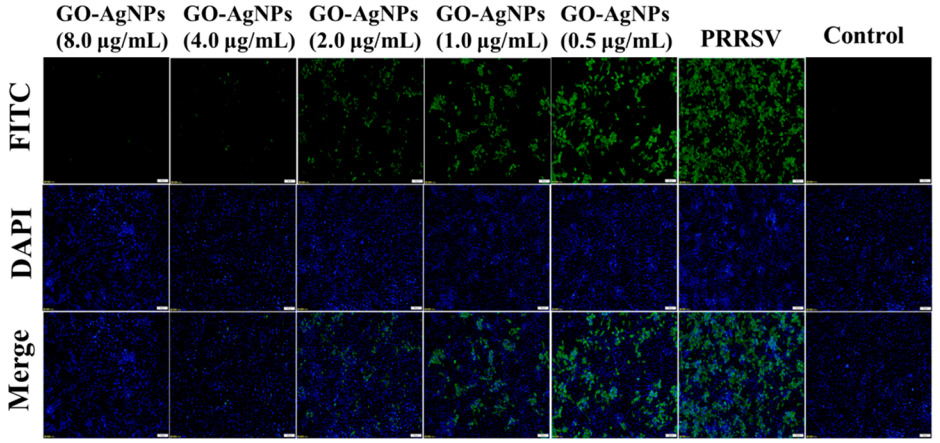

Figure 5. The indirect immunofluorescence assay was applied to analyze the infection of PRRSV cells with different concentrations of GO-AgNPs nanocomposites. Scale bar was 100 μm.

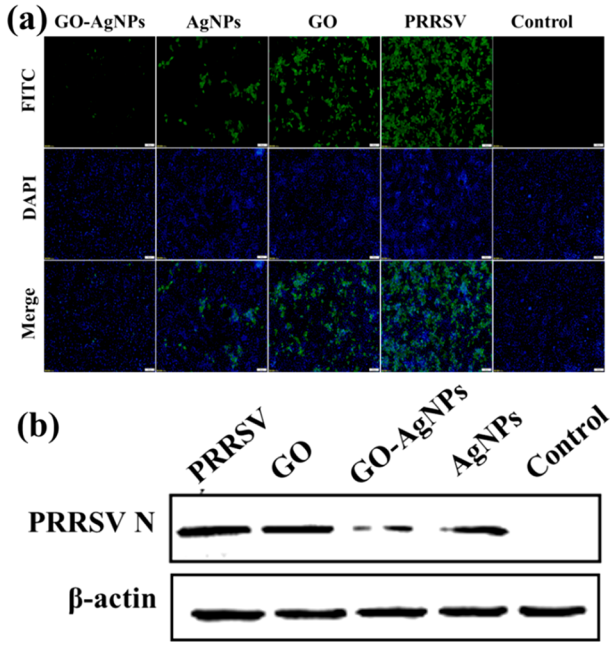

Figure 6. Inhibitory effects of GO-AgNPs nanocomposites, GO, and AgNPs against the virus. (a) Indirect immunofluorescence assay was used to analyze the MARC-145 cells infected with PRRSV after treatment with equal concentrations of GO-AgNPs nanocomposites, GO, and AgNPs. Scale bars were 100 μm. (b) Expression level of PRRSV N protein under GO-AgNPS, GO, and AgNPs exposure was analyzed by Western blot assays.

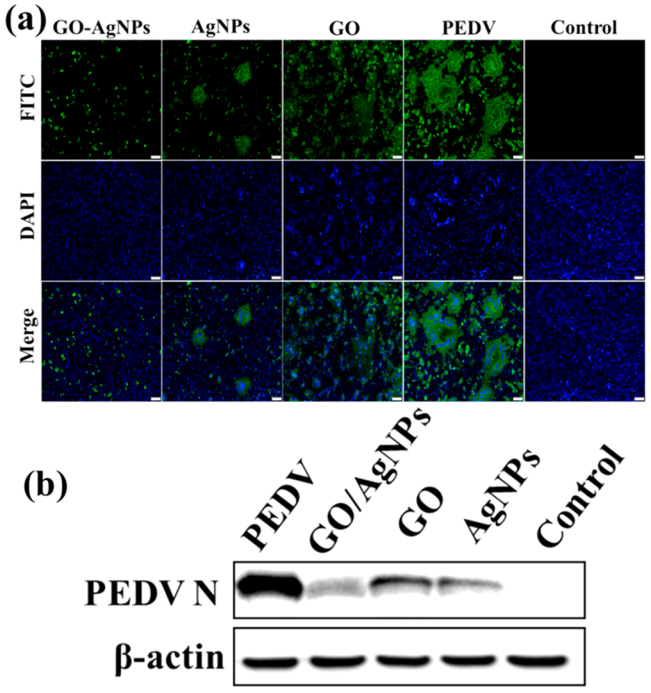

Figure 7. Inhibitory effects of GO-AgNPs nanocomposites, GO, and AgNPs against PEDV. (a) Indirect immunofluorescence assay was used to analyze the Vero cells infected with PEDV after exposure to equal concentrations of GO-AgNPs nanocomposites, GO, and AgNPs. Scale bars: 100 μm. (b) Western blotting detection of PEDV N protein expression in the presence of GO-AgNPs nanocomposites, GO, and AgNPs at 12 hpi.

self-assembly improved the inhibitory effect of GO and AgNPs largely. Figure 6b indicated that the PRRSV N protein expression levels in the experimental group were distinctly down-regulated, following the order GO-AgNPs nanocomposites > AgNPs > GO (Figure 6b). These consequences were line with the conclusion of indirect immunofluorescence.

3.4. Antiviral Activity of GO-AgNPs Nanocomposites on PEDV. To acquire the antiviral spectrum of GO-AgNPs nanocomposites, another RNA virus, PEDV (belonged to the family *Coronaviridae*), was selected. Similar to the results of PRRSV, the PEDV N protein expression level in the experimental group was remarkably down-regulated and the inhibitory effect was more pronounced under treatment with GO-AgNPs nanocomposites (Figure 7). Interestingly, with the concentration of GO-AgNPs nanocomposites increased, a gradual increase in the inhibition rate was observed (Figure S1). The results indicated that GO-AgNPs nanocomposites might be a potential broad-spectrum inhibitor and also have antiviral activity against other RNA viruses.

3.5. Mechanistic Considerations. The replication cycle of the virus usually follows three steps, namely, the initial entry and penetration into the host cell, then the replication and protein synthesis, and the budding of new virions.[46] To investigate the possible mechanism of GO-AgNPs nanocomposites in inhibiting PRRSV infection, plaque assays were conducted to detect the effect of GO-AgNPs nanocomposites on the entry of PRRSV. In the experimental

DOI: 10.1021/acsabm.8b00154
ACS Appl. Bio Mater. 2018, 1, 1286−1293

groups, PRRSV virions were cultured with various concentrations of GO-AgNPs nanocomposites prior to infection (1 h/37 °C). From Figure 8, it can be seen that the viral titers of

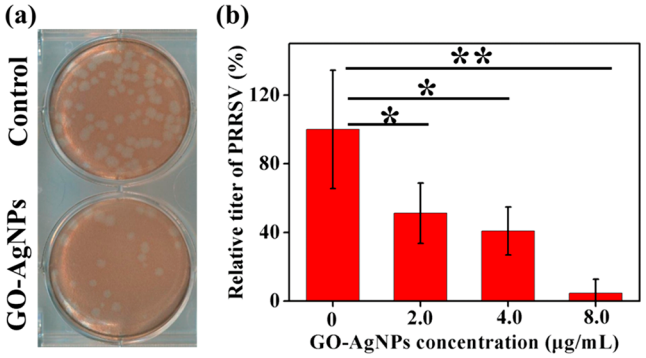

Figure 8. Effect of GO-AgNPs nanocomposites on the entry of PRRSV. (a) Plaque assays of the control and PRRSV pre-exposure with 4.0 μg/mL GO-AgNPs nanocomposites. (b) The influence of concentrations of GO-AgNPs nanocomposites on the relative titer of virus.

PRRSV were significantly reduced, indicating the strong antiviral activity of GO-AgNPs nanocomposites. Besides, it was found that the depression of viral titers was dependent on the concentration of GO-AgNPs nanocomposites. Compared to the control group, when the concentration of GO-AgNPs nanocomposites increased to 4.0 μg/mL, the relative titer of PRRSV was reduced to 40.8%. The early steps of interfering with the entry of the virus are reported to be feasible therapeutic tactics, since the acting site of the inhibitor is extracellular and relatively easy to obtain.[1] The results of plaque assays proved that GO-AgNPs nanocomposites could significantly inhibit PRRSV infection by directly inactivating the viruses before entering into the MARC-145 cells.

The natural immune response of the body, which prevents the virus from spreading from infected cells to adjacent uninfected cells, is the first line of defense against virus invasion. An important aspect of the natural immune response is the synthesis and secretion of type I interferon (α/β).[47] When host cells are infected by pathogens, they will be identified by the host's pattern recognition receptor. After activating a series of signal transduction within the cell, a number of transcription factors are activated, which cause the expression of interferon (IFN). The combining of IFN with the receptor on the cell membrane produces a series of interferon-stimulating genes (ISGs) through the JAK-STAT signaling pathway, which can directly inhibit the proliferation of the virus.[48,49] To investigate the underlying mechanism of GO-AgNPs nanocomposites antivirus, the effects of GO-AgNPs nanocomposites on the production of IFN-α and the ISGs were tested. Cells were exposed or unexposed with GO-AgNPs nanocomposites for 24 h, followed by extraction RNA via TRIzol reagent. As displayed in Figure 9, the effect of the experimental group treated with GO-AgNPs nanocomposites on IFN-α mRNA expression was 5.2 times that of the control group. (Figure 9a). Encouragingly, significant upregulation of interferon inducible protein 10 (IP-10) (Figure 9b), interferon-stimulated gene 56 (ISG-56) (Figure 9c), interferon-stimulated gene 54 (ISG-54) (Figure 9d), interferon-stimulated gene 20 (ISG-20) (Figure 9e), and interferon-stimulated gene 15 (ISG-15) (Figure 9f) was observed in the groups of MARC-145 cells exposed with GO-AgNPs nanocomposites. These results indicated that the inhibitory effect of GO-AgNPs nanocomposites may be attributed to the expression of IFN-α and ISGs. Additionally, there may be other antiviral mechanisms for the antiviral activity of GO-AgNPs nanocomposites.

4. CONCLUSION

In this study, GO-AgNPs nanocomposites with a good water solubility and high stability were successfully fabricated by the interfacial electrostatic self-assembly method. The antiviral activity of the as-prepared GO-AgNPs nanocomposites against PRRSV was investigated, and two possible molecular mechanisms were proposed. Detection of the titer and protein expression of virus showed that GO-AgNPs nanocomposites

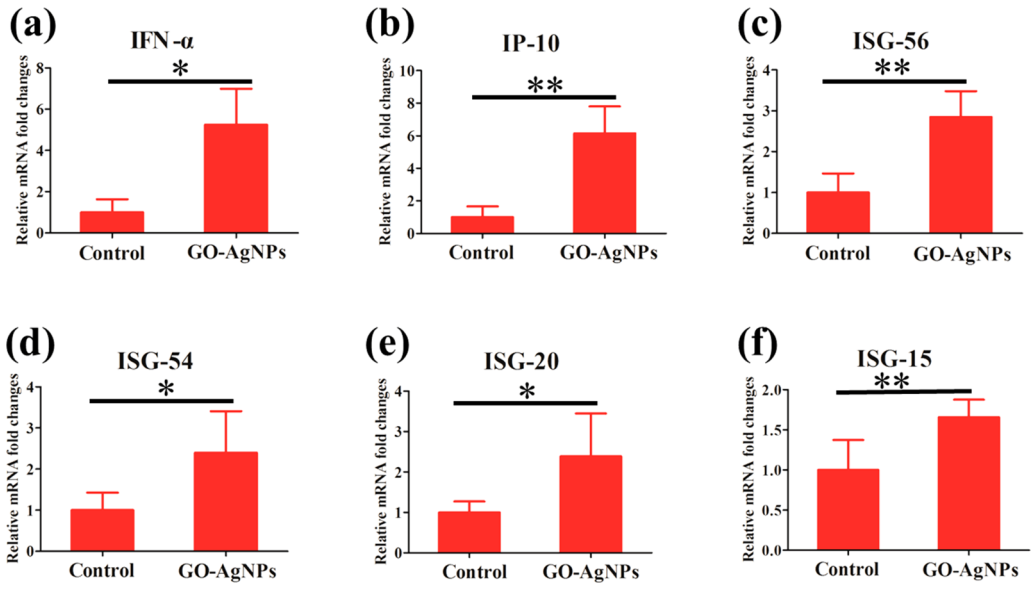

Figure 9. MRNA expressions of IFN-α (a), IP-10 (b), ISG-56 (c), ISG-54 (d), ISG-20 (e), and ISG-15 (f) in MARC-145 cells after exposure with or without GO-AgNPs nanocomposites.

DOI: 10.1021/acsabm.8b00154
ACS Appl. Bio Mater. 2018, 1, 1286−1293

had a stronger antiviral activity than AgNPs and GO at the same concentration. Besides, the experimental results showed that GO-AgNPs nanocomposites also had antiviral activity against PEDV (another RNA virus), which means that GO-AgNPs nanocomposites might be a broad-spectrum virus inhibitor. The plaque assays suggested that GO-AgNPs nanocomposites might inhibit virus entry into host cells, thereby suppressing virus replication. Furthermore, the activation of interferon-α and the up-regulated production of interferon stimulated genes might also play a viral role in the suppression of PRRSV infection. This work also provides theoretical references for antiviral researches of other nanocomposites.

■ ASSOCIATED CONTENT

Supporting Information

The Supporting Information is available free of charge on the ACS Publications website at DOI: 10.1021/acsabm.8b00154.

Materials and methods, instrument parameters, primer sequences used in qPCR, and indirect immunofluorescence assay (PDF)

■ AUTHOR INFORMATION

Corresponding Author

*E-mail: hyhan@mail.hzau.edu.cn.

ORCID

Shaobo Xiao: 0000-0003-0023-9188

Heyou Han: 0000-0001-9406-0722

Author Contributions

‖T.D. and J.L. contributed equally.

Notes

The authors declare no competing financial interest.

■ ACKNOWLEDGMENTS

This research was supported by the National Key R & D Program (2016YFD0500700), the National Natural Science Foundation of China (21778020 and 31672569), and the Scitech Innovation Foundation of Huazhong Agricultural University (2662017PY042).

■ REFERENCES

(1) Szunerits, S.; Barras, A.; Khanal, M.; Pagneux, Q.; Boukherroub, R. Nanostructures for the Inhibition of Viral Infections. *Molecules* **2015**, *20*, 14051−14081.

(2) Du, T.; Liang, J. G.; Dong, N.; Liu, L.; Fang, L. R.; Xiao, S. B.; Han, H. Y. Carbon Dots as Inhibitors of Virus by Activation of Type I Interferon Response. *Carbon* **2016**, *110*, 278−285.

(3) Barras, A.; Pagneux, Q.; Sane, F.; Wang, Q.; Boukherroub, R.; Hober, D.; Szunerits, S. High Efficiency of Functional Carbon Nanodots as Entry Inhibitors of Herpes Simplex Virus Type 1. *ACS Appl. Mater. Interfaces* **2016**, *8*, 9004−9013.

(4) Deokar, A. R.; Nagvenkar, A. P.; Kalt, I.; Shani, L.; Yeshurun, Y.; Gedanken, A.; Sarid, R. Graphene-Based "Hot Plate" for the Capture and Destruction of the Herpes Simplex Virus Type 1. *Bioconjugate Chem.* **2017**, *28*, 1115−1122.

(5) Villeret, B.; Dieu, A.; Straube, M.; Solhonne, B.; Miklavc, P.; Hamadi, S.; Le Borgne, R.; Mailleux, A.; Norel, X.; Aerts, J.; Diallo, D.; Rouzet, F.; Dietl, P.; Sallenave, J. M.; Garcia-Verdugo, I. Silver Nanoparticles Impair Retinoic Acid-Inducible Gene I-Mediated Mitochondrial Antiviral Immunity by Blocking the Autophagic Flux in Lung Epithelial Cells. *ACS Nano* **2018**, *12*, 1188−1202.

(6) Li, Y. H.; Lin, Z. F.; Zhao, M. Q.; Xu, T. T.; Wang, C. B.; Hua, L.; Wang, H. Z.; Xia, H. M.; Zhu, B. Silver Nanoparticle Based Codelivery of Oseltamivir to Inhibit the Activity of the H1N1 Influenza Virus through ROS-Mediated Signaling Pathways. *ACS Appl. Mater. Interfaces* **2016**, *8*, 24385−24393.

(7) Cagno, V.; Andreozzi, P.; D'Alicarnasso, M.; Silva, P. J.; Mueller, M.; Galloux, M.; Le Goffic, R.; Jones, S. T.; Vallino, M.; Hodek, J.; Weber, J.; Sen, S.; Janecek, E. R.; Bekdemir, A.; Sanavio, B.; Martinelli, C.; Donalisio, M.; Welti, M. A. R.; Eleouet, J. F.; Han, Y.; Kaiser, L.; Vukovic, L.; Tapparel, C.; Kral, P.; Krol, S.; Lembo, D.; Stellacci, F. Broad-Spectrum Non-Toxic Antiviral Nanoparticles with a Virucidal Inhibition Mechanism. *Nat. Mater.* **2017**, *17*, 195−203.

(8) Li, C. M.; Zheng, L. L.; Yang, X. X.; Wan, X. Y.; Wu, W. B.; Zhen, S. J.; Li, Y. F.; Luo, L. F.; Huang, C. Z. DNA-AuNP Networks on Cell Membranes as a Protective Barrier to Inhibit Viral Attachment, Entry and Budding. *Biomaterials* **2016**, *77*, 216−226.

(9) Baram Pinto, D.; Shukla, S.; Gedanken, A.; Sarid, R. Inhibition of HSV-1 Attachment, Entry, and Cell-to-Cell Spread by Functionalized Multivalent Gold Nanoparticles. *Small* **2010**, *6*, 1044−1050.

(10) Liga, M. V.; Maguireboyle, S. J.; Jafry, H. R.; Barron, A. R.; Li, Q. Silica Decorated TiO_2 for Virus Inactivation in Drinking Water-Simple Synthesis Method and Mechanisms of Enhanced Inactivation Kinetics. *Environ. Sci. Technol.* **2013**, *47*, 6463−6470.

(11) Ziem, B.; Azab, W.; Gholami, M. F.; Rabe, J. P.; Osterrieder, N.; Haag, R. Size-Dependent Inhibition of Herpesvirus Cellular Entry by Polyvalent Nanoarchitectures. *Nanoscale* **2017**, *9*, 3774−3783.

(12) Kwon, S. J.; Na, D. H.; Kwak, J. H.; Douaisi, M.; Zhang, F.; Park, E. J.; Park, J. H.; Youn, H.; Song, C. S.; Kane, R. S.; Dordick, J. S.; Lee, K. B.; Linhardt, R. J. Nanostructured Glycan Architecture is Important in the Inhibition of Influenza A Virus Infection. *Nat. Nanotechnol.* **2016**, *12*, 48−54.

(13) Yang, X. X.; Li, C. M.; Huang, C. Z. Curcumin Modified Silver Nanoparticles for Highly Efficient Inhibition of Respiratory Syncytial Virus Infection. *Nanoscale* **2016**, *8*, 3040−3048.

(14) Zhang, M.; Zhao, Y.; Yan, L.; Peltier, R.; Hui, W.; Yao, X.; Cui, Y.; Chen, X.; Sun, H.; Wang, Z. Interfacial Engineering of Bimetallic Ag/Pt Nanoparticles on Reduced Graphene Oxide Matrix for Enhanced Antimicrobial Activity. *ACS Appl. Mater. Interfaces* **2016**, *8*, 8834−8840.

(15) Galdiero, S.; Falanga, A.; Vitiello, M.; Cantisani, M.; Marra, V.; Galdiero, M. Silver Nanoparticles as Potential Antiviral Agents. *Molecules* **2011**, *16*, 8894−8918.

(16) Akbarzadeh, A.; Kafshdooz, L.; Razban, Z.; Dastranj Tbrizi, A.; Rasoulpour, S.; Khalilov, R.; Kavetskyy, T.; Saghfi, S.; Nasibova, A. N.; Kaamyabi, S.; Kafshdooz, T. An Overview Application of Silver Nanoparticles in Inhibition of Herpes Simplex Virus. *Artif. Cells, Nanomed., Biotechnol.* **2018**, *46*, 263−267.

(17) Baram-Pinto, D.; Shukla, S.; Perkas, N.; Gedanken, A.; Sarid, R. Inhibition of Herpes Simplex Virus Type 1 Infection by Silver Nanoparticles Capped with Mercaptoethane Sulfonate. *Bioconjugate Chem.* **2009**, *20*, 1497−1502.

(18) Lu, L.; Sun, R. W. Y.; Chen, R.; Hui, C. K.; Ho, C. M.; Luk, J. M.; Lau, G. K. K.; Che, C. M. Silver Nanoparticles Inhibit Hepatitis B Virus Replication. *Antivir. Ther.* **2008**, *13*, 253−262.

(19) Khandelwal, N.; Kaur, G.; Kumar, N.; Tiwari, A. Application of Silver Nanoparticles in Viral Inhibition: A New Hope for Antivirals. *Dig. J. Nanomater. Bios.* **2014**, *9*, 175−186.

(20) Stark, W. J. Nanoparticles in Biological Systems. *Angew. Chem., Int. Ed.* **2011**, *50*, 1242−1258.

(21) Danilczuk, M.; Lund, A.; Sadlo, J.; Yamada, H.; Michalik, J. Conduction Electron Spin Resonance of Small Silver Particles. *Spectrochim. Acta, Part A* **2006**, *63*, 189−191.

(22) Lv, M.; Su, S.; He, Y.; Huang, Q.; Hu, W.; Li, D.; Fan, C.; Lee, S. T. Long-Term Antimicrobial Effect of Silicon Nanowires Decorated with Silver Nanoparticles. *Adv. Mater.* **2010**, *22*, 5463−5467.

(23) Ye, S.; Shao, K.; Li, Z.; Guo, N.; Zuo, Y.; Li, Q.; Lu, Z.; Chen, L.; He, Q.; Han, H. Antiviral Activity of Graphene Oxide: How Sharp Edged Structure and Charge Matter. *ACS Appl. Mater. Interfaces* **2015**, *7*, 21571−21579.

(24) Sametband, M.; Kalt, I.; Gedanken, A.; Sarid, R. Herpes Simplex Virus Type-1 Attachment Inhibition by Functionalized Graphene Oxide. *ACS Appl. Mater. Interfaces* **2014**, *6*, 1228−1235.
(25) Munoz, A.; Sigwalt, D.; Illescas, B. M.; Luczkowiak, J.; Rodriguez-Perez, L.; Nierengarten, I.; Holler, M.; Remy, J. S.; Buffet, K.; Vincent, S. P.; Rojo, J.; Delgado, R.; Nierengarten, J. F.; Martin, N. Synthesis of Giant Globular Multivalent Glycofullerenes as Potent Inhibitors in a Model of Ebola Virus Infection. *Nat. Chem.* **2016**, *8*, 50−57.
(26) Yang, X. X.; Li, C. M.; Li, Y. F.; Wang, J.; Huang, C. Z. Synergistic Antiviral Effect of Curcumin Functionalized Graphene Oxide against Respiratory Syncytial Virus Infection. *Nanoscale* **2017**, *9*, 16086−16092.
(27) Premkumar, T.; Geckeler, K. E. Graphene-DNA Hybrid Materials: Assembly, Applications, and Prospects. *Prog. Polym. Sci.* **2012**, *37*, 515−529.
(28) Chowdhury, I.; Duch, M. C.; Mansukhani, N. D.; Hersam, M. C.; Bouchard, D. Interactions of Graphene Oxide Nanomaterials with Natural Organic Matter and Metal Oxide Surfaces. *Environ. Sci. Technol.* **2014**, *48*, 9382−9390.
(29) Lin, Y.; Jin, J.; Song, M. Preparation and Characterisation of Covalent Polymer Functionalized Graphene Oxide. *J. Mater. Chem.* **2011**, *21*, 3455−3461.
(30) Bai, S.; Shen, X. Graphene-Inorganic Nanocomposites. *RSC Adv.* **2012**, *2*, 64−98.
(31) Sun, L.; Du, T.; Hu, C.; Chen, J.; Lu, J.; Lu, Z.; Han, H. Antibacterial Activity of Graphene Oxide/g-C_3N_4 Composite through Photocatalytic Disinfection under Visible Light. *ACS Sustainable Chem. Eng.* **2017**, *5*, 8693−8701.
(32) Chen, J.; Sun, L.; Cheng, Y.; Lu, Z.; Shao, K.; Li, T.; Hu, C.; Han, H. Graphene Oxide-Silver Nanocomposite: Novel Agricultural Antifungal Agent against Fusarium Graminearum for Crop Disease Prevention. *ACS Appl. Mater. Interfaces* **2016**, *8*, 24057−24070.
(33) Cruz, J. L. G.; Zuniga, S.; Becares, M.; Sola, I.; Ceriani, J. E.; Juanola, S.; Plana, J.; Enjuanes, L. Vectored Vaccines to Protect against PRRSV. *Virus Res.* **2010**, *154*, 150−160.
(34) Hummers, W. S.; Offeman, R. E. Preparation of Graphitic Oxide. *J. Am. Chem. Soc.* **1958**, *80*, 1339−1339a.
(35) Lee, P. C.; Meisel, D. Adsorption and Surface-Enhanced Raman of Dyes on Silver and Gold Sols. *J. Phys. Chem.* **1982**, *86*, 3391−3395.
(36) Ren, W.; Fang, Y.; Wang, E. A Binary Functional Substrate for Enrichment and Ultrasensitive SERS Spectroscopic Detection of Folic Acid Using Graphene Oxide/Ag Nanoparticle Hybrids. *ACS Nano* **2011**, *5*, 6425−6433.
(37) Luo, R.; Fang, L.; Jin, H.; Jiang, Y.; Wang, D.; Chen, H.; Xiao, S. Antiviral Activity of Type I and Type III Interferons against Porcine Reproductive and Respiratory Syndrome Virus (PRRSV). *Antiviral Res.* **2011**, *91*, 99−101.
(38) Duan, E.; Wang, D.; Fang, L.; Ma, J.; Luo, J.; Chen, H.; Li, K.; Xiao, S. Suppression of Porcine Reproductive and Respiratory Syndrome Virus Proliferation by Glycyrrhizin. *Antiviral Res.* **2015**, *120*, 122−125.
(39) Xu, C.; Wang, X.; Zhu, J. W. Graphene-Metal Particle Nanocomposites. *J. Phys. Chem. C* **2008**, *112*, 19841−19845.
(40) Paredes, J. I.; Villarrodil, S.; Martínezalonso, A.; Tascón, J. M. Graphene Oxide Dispersions in Organic Solvents. *Langmuir* **2008**, *24*, 10560−10564.
(41) Xu, C.; Wang, X. Fabrication of Flexible Metal Nanoparticle Films Using Graphene Oxide Sheets as Substrates. *Small* **2009**, *5*, 2212−2217.
(42) Fan, Z. J.; Kai, W.; Yan, J.; Wei, T.; Zhi, L. J.; Feng, J.; Ren, Y. M.; Song, L. P.; Wei, F. Facile Synthesis of Graphene Nanosheets via Fe Reduction of Exfoliated Graphite Oxide. *ACS Nano* **2011**, *5*, 191−198.
(43) De Faria, A. F.; Martinez, D. S.; Meira, S. M.; de Moraes, A. C.; Brandelli, A.; Filho, A. G.; Alves, O. L. Anti-Adhesion and Antibacterial Activity of Silver Nanoparticles Supported on Graphene Oxide Sheets. *Colloids Surf., B* **2014**, *113*, 115−124.
(44) Huang, Q.; Wang, J.; Wei, W.; Yan, Q.; Wu, C.; Zhu, X. A Facile and Green Method for Synthesis of Reduced Graphene Oxide/Ag Hybrids as Efficient Surface Enhanced Raman Scattering Platforms. *J. Hazard. Mater.* **2015**, *283*, 123−130.
(45) Zhang, H. J.; Chen, Y. L.; Liang, M. J.; Xu, L. F.; Qi, S. D.; Chen, H. L.; Chen, X. G. Solid-Phase Synthesis of Highly Fluorescent Nitrogen-Doped Carbon Dots for Sensitive and Selective Probing Ferric Ions in Living Cells. *Anal. Chem.* **2014**, *86*, 9846−9852.
(46) Von Itzstein, M. The War against Influenza: Discovery and Development of Sialidase Inhibitors. *Nat. Rev. Drug Discovery* **2007**, *6*, 967−974.
(47) Schoggins, J. W. Interferon-Stimulated Genes: Roles in Viral Pathogenesis. *Curr. Opin. Virol.* **2014**, *6*, 40−46.
(48) Fensterl, V.; Sen, G. C. Interferon-Induced I Fit Proteins: Their Role in Viral Pathogenesis. *J. Virol.* **2015**, *89*, 2462−2468.
(49) Schoggins, J. W.; Wilson, S. J.; Panis, M.; Murphy, M. Y.; Jones, C. T.; Bieniasz, P.; Rice, C. M. A Diverse Range of Gene Products are Effectors of the Type I Interferon Antiviral Response. *Nature* **2011**, *472*, 481−485.

DOI: 10.1021/acsabm.8b00154
ACS Appl. Bio Mater. 2018, 1, 1286−1293